Upper mantle thermal variations beneath the Transantarctic Mountains inferred from teleseismic S-wave attenuation

Jesse F. Lawrence,[1,2] Douglas A. Wiens,[1] Andrew A. Nyblade,[3]
Sridhar Anandakrishan,[3] Patrick J. Shore,[1] and Donald Voigt[3]

Received 30 August 2005; revised 9 November 2005; accepted 15 November 2005; published 2 February 2006.

[1] This study examines teleseismic S-wave attenuation variations between the Ross Sea in West Antarctica and Vostok Subglacial Highlands in East Antarctica. These analyses indicate that δt^* is $\sim$1 second greater beneath the Ross Sea than East Antarctica, with the transition occurring beneath the Transantarctic Mountains. While the structure is non-unique, low attenuation beneath East Antarctica is consistent with thick subcontinental lithosphere ($\geq$250 km) and negligible asthenosphere. In contrast, the Ross Sea possesses a thin lithosphere underlain by thick, highly anelastic asthenosphere. Independent temperature estimates from velocity and quality factor indicate that the mantle is 200–400°C colder beneath East Antarctica than the Ross Sea between 80 and 220 km depth. The temperature variation beneath the Transantarctic Mountains may have assisted in the asymmetric uplift of the mountains. Attenuation and velocity anomalies within East Antarctica may delineate regions of elevated temperature, representing recently modified sections between older lithospheric blocks. **Citation:** Lawrence, J. F., D. A. Wiens, A. A. Nyblade, S. Anandakrishan, P. J. Shore, and D. Voigt (2006), Upper mantle thermal variations beneath the Transantarctic Mountains inferred from teleseismic S-wave attenuation, *Geophys. Res. Lett.*, *33*, L03303, doi:10.1029/2005GL024516.

1. Introduction

[2] The Transantarctic Mountains (TAMs), a 200-km wide, 4-km high mountain range, define the 4000-km boundary between East Antarctica (EA) and West Antarctica (WA). Surface wave studies show that upper mantle seismic velocities sharply decrease from EA to WA beneath the TAMs [*Ritzwoller et al.*, 2001; *Danesi and Morelli*, 2001; J. F. Lawrence et al., Rayleigh wave phase velocity analysis of the Transantarctic Mountains, West Antarctica Rift System, and East Antarctica, submitted to *Journal of Geophysical Research*, 2005, hereinafter referred to as Lawrence et al., submitted manuscript, 2005]. This velocity dichotomy is often presented as evidence for a thermal boundary between the colder Precambrian EA craton and the warmer Mesozoic to Cenozoic WA mantle [*Tingey*, 1991]. Cretaceous to Cenozoic extension in the Ross Sea (RS) [*Behrendt*, 1999] was likely accompanied by thinning and reworking of the lithosphere and asthenosphere [*Busetti et al.*, 1999] causing elevated heat flow [*Blackman et al.*, 1987; *Berg et al.*, 1989] and volcanism [*LeMasurier and Thomson*, 1989]. Nevertheless, studies examining solely seismic velocity can rarely differentiate between thermal and chemical anomalies, leading to ambiguous interpretation.

[3] Experimental results show that seismic attenuation is highly sensitive to temperature [*Jackson et al.*, 1992, 2002]. Inverse correlation between seismic velocity and attenuation most likely indicates thermal variations in the mantle. This study investigates lateral variation in shear-wave attenuation beneath the Transantarctic Mountain Seismic Experiment (TAMSEIS), which deployed 41 broadband seismometers between the RS and the Vostok Subglacial Highlands in EA (Figure 1). These data also provided high-resolution images of mantle seismic velocities [*Watson*, 2005; Lawrence et al., submitted manuscript, 2005]. Based on attenuation variations we estimate lateral quality factor (Q) and temperature contrasts between EA and WA.

2. Data and Method

[4] This study employs three-component, broadband seismic data recorded at 44 seismic stations (41 TAMSEIS and 3 GSN stations) in Antarctica between November 2000 and December 2003. The data are limited to high signal-to-noise records from large earthquakes (>6.0 mb) and distances between 45 and 80°. This distance range ensures that *S*-waves arrive separate from other phases (e.g., *SS*). Tangential records are analyzed to avoid *P-SV* scattering from 2D and 3D structure and interference due simultaneously arriving *SKS* waves. Prior to analysis each waveform is instrument response corrected, rotated, de-trended, band-passed (0.02–0.10 Hz), windowed (40 seconds), tapered (10%), and padded with zeros.

[5] Individual differential attenuation measurements, δt^*, are calculated from the slopes of the spectral transfer functions between pairs of *S*-waves from the same earthquake after *Flanagan and Wiens* [1994]. Each interstation measurement is corrected for path length by removing the δt^* value predicted by PREM [*Dziewonski and Anderson*, 1981], which is small (<0.2s) for short interstation distances ($\Delta < 13°$). With $N(N-1)/2$ interstation measurements for each earthquake, where N is the number of stations, we employ the inversion method typically applied to the multi-channel cross-correlation [*vanDecar and Crosson*, 1990; *Venkataraman et al.*, 2004] to calculate relative attenuation at each station. The sum of the anomalies is set to zero ($\Sigma\delta t^* = 0$), so attenuation residuals are relative to a regional

[1]Department of Earth and Planetary Sciences, Washington University, St. Louis, Missouri, USA.
[2]Now at Institute of Geophysics and Planetary Physics, Scripps Institution of Oceanography, La Jolla, California, USA.
[3]Department of Geosciences, Pennsylvania State University, University Park, Pennsylvania, USA.

0094-8276/06/2005GL024516$05.00

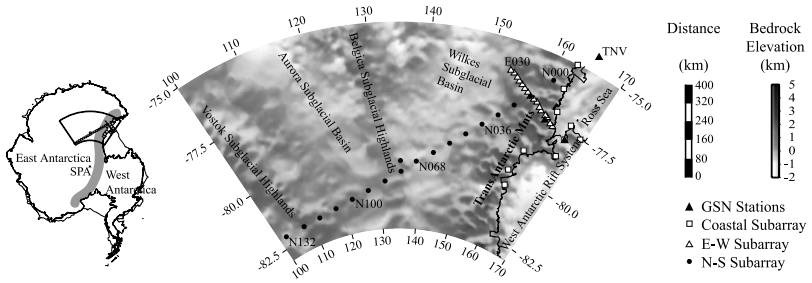

Figure 1. A map of the seismic stations overlain on shaded relief bedrock topography [*Lythe et al.*, 2001].

mean. The δt^* measurements from all usable earthquakes are averaged to stabilize δt^* estimates for each station.

[6] Differential attenuation, δt^*, is equal to the difference in t^* values,

$$t^* = \int_{path} Q^{-1} dt \tag{1}$$

accumulated along the raypaths to the two stations. δt^* is largely sensitive to quality factor (Q) structure where the raypaths diverge, removing effects of the source spectrum and near-source attenuation. In practice, δt^* is mostly sensitive to the high attenuation of the asthenosphere, where Q is low. Additionally, averaging three or more (typically 8 or more) results from multiple earthquakes with varying back azimuths reduces sensitivity farther from the stations. Thus, we may assume the final δt^* estimates reflect the attenuation structure of the upper 300–400 km beneath each station relative to the regional average.

3. Results

[7] The δt^* values are ~1s higher beneath the Ross Sea and the TAMs than beneath EA (Figure 2). The highest relative attenuation ($\delta t^* = +0.8$ s) occurs beneath Ross Island. The lowest relative attenuation ($\delta t^* = -1.1$ s) occurs ~200 km inland at N028 and at the south-west end of the array at N132. The transition from high to low δt^* occurs 100 ± 50 km inland from the coast. Within EA, elevated attenuation ($\delta t^* > 0.1$ s) accumulates beneath the Belgica and Vostok Subglacial Highlands. Near zero δt^* occurs beneath the Wilkes Subglacial Basin. The relative attenuation is inversely proportional to regional phase velocity (Lawrence et al., submitted manuscript, 2005) (Figure 2) and body wave [*Watson*, 2005] anomalies.

4. Attenuation/Q Modeling

[8] The attenuation variation between EA and WA in the Ross Island region (~1 second) can be modeled as structural variations in upper mantle Q. We calculate theoretical δt^* values for various models of upper mantle Q structure by integrating equation (1) from 0 to 400 km using a ray parameter of 11.8 s deg^{-1}. We then compare these values with observations near the dense EW-subarray extending from Ross Island to the Wilkes Subglacial Basin.

[9] δt^* is insensitive to the depth of an attenuating layer, so models determined from these data are non-unique. However, because δt^* values are relatively insensitive to high-Q lithosphere and mid-mantle, we model attenuation by varying asthenospheric thickness and quality factor. Global 1D Q models [e.g., *Dziewonski and Anderson*, 1981; *Widmer et al.*, 1991] demonstrate a pattern of low lithospheric attenuation ($300 < Q_L < 600$), high asthenospheric attenuation ($Q_A \sim 80$), and intermediate mid-mantle attenuation ($Q_M \sim 143$). We model attenuation variations with two end-member cases; 1) quality factor varies or 2) layer thickness varies. Theoretical attenuation residuals are calculated for lithospheric and asthenospheric variation in quality factor and layer thickness (Figure 3). These end members indicate which models can provide a good fit to the data.

[10] Case 1: The relative attenuation anomalies (~1 s) are reproducible by large, but reasonable variations in Q within a constant thickness layer (80 to 220 km depth and $30 < Q < 600$). A smooth curve is fit to the relative attenuation as a function of distance from the coast (Figure 4a). Grid searches are conducted at 50 evenly spaced distances from the coast to determine which Q models best fit each distance. The result is a 2D variable Q profile with constant layer thickness (Figure 4b). Because the measurements are relative, the solution is non-unique. Nevertheless, bounds can be placed on Q. It is unreasonable for Q to be higher than Q_L within the asthenospheric depth range. Therefore, upper bounds are given by EA $Q = 600 \pm 100$ and RS $Q = 35 \pm 2$. Lower EA Q values give rise to RS Q values even lower than 35. An alternate scenario includes less extreme Q variations in both of the upper two layers (e.g., $150 < Q_L < 600$ and $32 < Q_A < 150$).

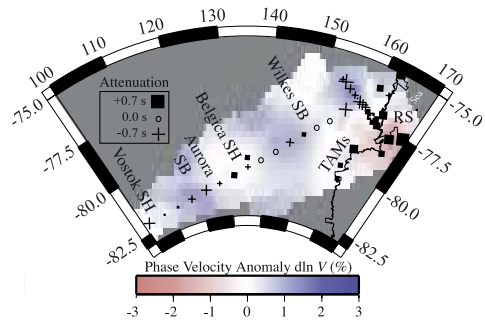

Figure 2. The geographic distribution of average relative attenuation plotted at each station overlain on a 120-second phase velocity map (Lawrence et al., submitted manuscript, 2005). Regional features such as subglacial highlands (SH) and basins (SB) are identified for geographic reference.

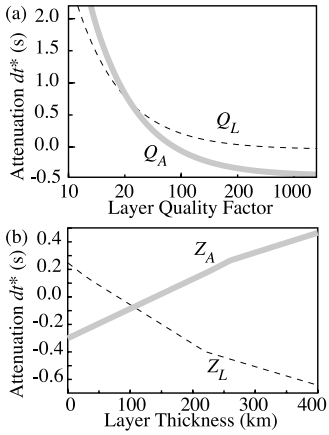

Figure 3. Theoretical attenuation resultant from varying asthenospheric (grey solid) and lithospheric (black dashed) (a) quality factor and (b) layer thickness, calculated by integrating Q^{-1} from 0 to 400 km with a slowness of 11.8 s deg^{-1}.

[11] Case 2: The observed δt^* variations are also reproducible by contrasting extremely thick lithosphere ($Z_L \sim$ 350 km) beneath EA with extremely thick asthenosphere ($Z_A \sim$ 350 km) beneath the RS, given constant-Q layers with Q given by PREM. Thinning either EA lithosphere or RS asthenosphere would require the other region to be thicker, which is unlikely as discussed below. A set of grid searches yields a 2D variable layer thickness profile (Figure 4c) from the 1D models shown in Figure 3b. Beneath the TAMs the lithosphere and asthenosphere thin in opposite directions, reaching $Z_A = 0$ at 150 ± 10 km from the coast and $Z_L = 0$ at 50 ± 30 km inland. Thus, the major variation in structure occurs at 100 ± 50 km inland from the coast.

[12] Solutions combining both variable Q and variable layer thickness are more realistic than either end member. Despite the non-uniqueness, the end-members are similar, suggesting that EA has lithospheric Q values in the asthenospheric depth range, and has no anelastic layer. It is unlikely that RS asthenosphere or EA lithosphere extend to below 350 km because the velocity differences diminish below 250 km [*Ritzwoller et al.*, 2001; Lawrence et al., submitted manuscript, 2005] and attenuation correlates with velocity. Thinner Z_L and Z_A limits (<250 km) require lower RS Q_A values (<50).

5. Temperature Estimation

[13] The observed attenuation dichotomy between EA and the RS has important implications for upper mantle thermal structure. Temperature, T, and Q are related through a frequency and grain size dependent power law [e.g., *Jackson et al.*, 1992, 2002]. The frequency band is constant and we assume negligible grain size variation, so the power law relation simplifies to,

$$T_2 = [1/T_1 - R/(E\alpha)\ln(Q_2/Q_1)]^{-1}, \quad (2)$$

where the frequency dependence is $\alpha = 0.26$, activation entropy is $E = 424$ kJ/mol, and R is the gas constant. The average temperature is set to $T = 1400$°K. Consequently, a transition from EA $Q = 600 \pm 100$ to RS $Q = 35 \pm 2$ requires a temperature increase of $\Delta T = 416 \pm 50$°K. Assuming a reasonable grain size (10 mm) and depth (120 km) in the mantle provides temperature estimates of 1000°C for Q_A = 600 and 1400°C for $Q_A = 35$ [*Jackson et al.*, 2002; *Faul and Jackson*, 2005]. If both Q_L and Q_A change from EA to RS, temperature variation from equation (2) minimize at ΔT = 210 ± 30°K with a model having EA $Q_L = 600$ and Q_A = 125 and RS Q_L = 125 and Q_A = 33. An intermediate temperature variation ($\Delta T = 310 \pm 50$°K) is required for a variable Q and thickness end-member model ($50 < Q < 600$) limited to the upper 250 km.

[14] The estimated upper mantle temperature variation between EA and the RS is consistent with seismic velocity variations from surface wave studies, which show that the RS shear-wave velocity is 7–8% slower than EA between 80 and 220 km depth [*Ritzwoller et al.*, 2001; Lawrence et al., submitted manuscript, 2005]. The temperature dependent anharmonic velocity perturbation is -8.5×10^{-5} K^{-1} [*Anderson and Isaak*, 1995]. The anelastic contribution to seismic velocity is $-7.4 \times 10^{-3}\ Q^{-1}$ K^{-1} at a pressure of 4 GPa (120 km depth) [*Jackson et al.*, 2002; *Faul and Jackson*, 2005]. Assuming $Q_A = 80$ yields a net velocity perturbation of $\partial \ln V_S / \partial T = -1.8 \times 10^{-4}$ K^{-1}. The observed variation in shear velocity from EA to the RS, ($\delta \ln V_S$ = −7%) requires a temperature increase of $\Delta T = 400$.

[15] Within East Antarctica lateral δt^* and velocity anomalies with opposite sign suggest possible small-scale thermal anomalies (Figure 2). Velocity and Q anomalies within EA are smaller than those between EA and WA. The highest temperature anomalies estimated from 120-second phase velocities (Lawrence et al., submitted manuscript, 2005) are $\Delta T = 150 \pm 50$°K located beneath the Belgica Subglacial Highlands. The corresponding temperature in-

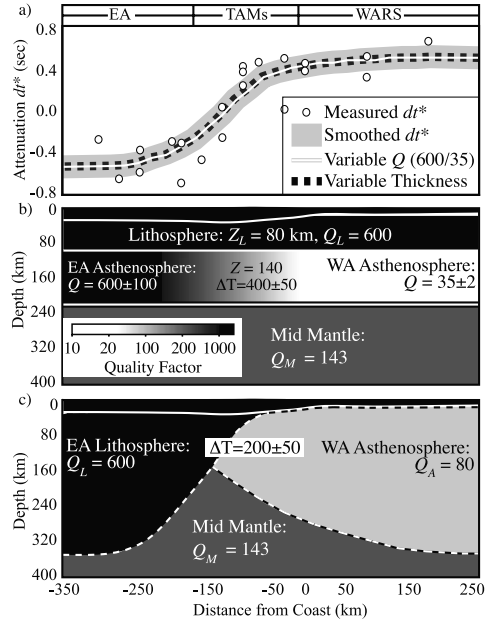

Figure 4. (a) A smoothed 2D representation (grey line) of δt^* (squares) near the E-W subarray, excluding 3 outliers, is fit by 2D models having variable (b) quality factor (white line) or (c) layer thickness (dashed line).

crease estimated from attenuation is $\Delta T = 190 \pm 50$°K. This thermal variation may represent lithospheric reworking and may be the result of Proterozoic tectonic activity in East Antarctica [*Studinger et al.*, 2003].

6. Discussion

[16] We observe inversely correlated changes in upper mantle seismic velocity and attenuation between EA and RS, and to a lesser extent within EA. These anomalies are not likely due to chemical heterogeneity, such as iron depletion in continental lithosphere, because attenuation is relatively insensitive to compositional variation [e.g., *Faul and Jackson*, 2005]. Although water increases attenuation and decreases velocity [*Karato*, 2003], the TAMs and RS have not been located near subduction since the Ross Orogeny, ~500 Ma [*Tingey*, 1991] and should be generally anhydrous. While crustal scattering can cause some attenuation-like waveform effects, these phenomena are generally only significant at much higher frequencies than used in this study, and will not correlate with velocity structure [*Flanagan and Wiens*, 1994]. Thus the results support the hypothesis that EA has a colder, deeper root than WA.

[17] The seismic velocity and Q variations indicate that EA has a 200–400°K colder and ~1% denser mantle than the West Antarctic (with thermal expansion coefficient, $\alpha_{th} = 3.5 \times 10{-}5\ K^{-1}$). These findings are consistent with Tanzania, where low-Q_A is found beneath rifting adjacent to a high-Q_A craton [*Venkataraman et al.*, 2004]. The transition from cold and dense to warm, anelastic, and less dense beneath the crest of the TAMs (100 ± 50 km from the coast), has considerable implications for the geodynamics governing tectonics in the region. Lower density beneath the mountain front likely aided in the asymmetric uplift of the TAMs [*Fitzgerald*, 1992] by providing a buoyant load [*ten Brink et al.*, 1997]. The large variations in lithospheric and asthenospheric thicknesses and temperatures suggest large differences in the mechanical behavior of EA and WA, which are important for understanding RS extension, TAM uplift, and present-day postglacial rebound.

[18] **Acknowledgments.** We thank everyone who assisted in deploying and retrieving TAMSEIS stations and data. IRIS PASSCAL and DMC provided portable seismic instrumentation and data support. USGS is thanked for maintaining the GSN stations used here. Maps were generated using Generic Mapping Tools. This research was supported by NSF grants OPP9909603 and OPP9909648.

References

Anderson, O. L., and D. G. Isaak (1995), Elastic constants of mantle minerals at high temperature, in *A Handbook of Physical Constants: Mineral Physics and Crystallography*, vol. 2, edited by T. J. Ahrens, pp. 64–97, AGU, Washington, D. C.

Behrendt, J. C. (1999), Crustal and lithospheric structure of the West Antarctic Rift System from geophysical investigations—A review, *Global Planet. Change*, *23*, 25–44.

Berg, J. H., R. J. Moscati, and D. L. Herz (1989), A petrologic geotherm from a continental rift in Antarctica, *Earth Planet. Sci. Lett.*, *93*, 98–108.

Blackman, D. K., R. P. Von Herzen, and L. A. Lawver (1987), Heat flow and tectonics in the western Ross Sea, Antarctica, in *The Antarctic Continental Margin: Geology and Geophysics of the Western Ross Sea*, edited by F. J. Davey, pp. 179–189, Circum-Pac. Counc. for Energy and Nat. Resour., Houston, Tex.

Busetti, M., G. Spadini, F. M. Van der Wateren, S. Cloetingh, and C. Zanolla (1999), Kinematic modeling of the West Antarctic Rift System, Ross Sea, Antarctica, in *Global and Planetary Change*, edited by S. A. P. L. Cloetingh, pp. 79–103, Elsevier, New York.

Danesi, S., and A. Morelli (2001), Structure of the upper mantle under the Antarctic Plate from surface wave tomography, *Geophys. Res. Lett.*, *28*, 4395–4398.

Dziewonski, A. M., and D. L. Anderson (1981), Preliminary reference Earth model, *Phys. Earth Planet. Inter.*, *25*, 297–356.

Fitzgerald, P. G. (1992), The Transantarctic Mountains of southern Victoria Land: The application of apatite fission track analysis to a rift shoulder uplift, *Tectonics*, *11*, 634–662.

Faul, U. H., and I. Jackson (2005), The seismological signature of temperature and grain size variations in the upper mantle, *Earth Planet. Sci. Lett.*, *234*, 119–134.

Flanagan, M. P., and D. A. Wiens (1994), Radial upper mantle attenuation structure of inactive back arc basin differential shear wave measurements, *J. Geophys. Res.*, *99*, 15,469–15,485.

Jackson, I., M. S. Paterson, and J. D. Fitz Gerald (1992), Seismic wave dispersion and attenuation in Aheim dunite: An experimental study, *Geophys. J. Int.*, *108*, 517–534.

Jackson, I., J. D. Fitz Gerald, U. H. Faul, and B. H. Tan (2002), Grain-size-sensitive seismic wave attenuation in polycrystaline olivine, *J. Geophys. Res.*, *107*(B12), 2360, doi:10.1029/2001JB001225.

Karato, S.-I. (2003), Mapping water content in the upper mantle, in *Inside the Subduction Factory*, *Geophys. Monogr. Ser.*, vol. 138, edited by J. M. Eiler, pp. 135–152, AGU, Washington, D. C.

LeMasurier, W. E., and J. W. Thomson (Eds.) (1989), *Volcanoes of the Antarctic Plate and Southern Oceans*, *Antarct. Res. Ser.*, vol. 48, AGU, Washington, D. C.

Lythe, M. B., D. G. Vaughan, and B. Consortium (2001), BEDMAP: A new ice thickness and subglacial topographic model of Antarctica, *J. Geophys. Res.*, *106*, 11,335–11,351.

Ritzwoller, M. H., N. M. Shapiro, A. L. Levshin, and G. M. Leahy (2001), Crustal and upper mantle structure beneath Antarctica and surrounding oceans, *J. Geophys. Res.*, *106*, 30,645–30,670.

Studinger, M., et al. (2003), Geophysical models for the tectonic framework of the Lake Vostok region, East Antarctica, *Earth Planet. Sci. Lett.*, *205*, 195–210.

ten Brink, U. T., R. I. Hackney, S. Bannister, T. A. Stern, and Y. Makovsky (1997), Uplift of the Transantarctic Mountains and the bedrock beneath the East Antarctic ice sheet, *J. Geophys. Res.*, *102*, 27,603–27,621.

Tingey, R. J. (1991), *The Geology of Antarctica*, 680 pp., Clarendon, Oxford, U. K.

vanDecar, J. C., and R. S. Crosson (1990), Determination of teleseismic relative phase arrival times using multi-channel cross correlation and least squares, *Bull. Seismol. Soc. Am.*, *80*, 150–169.

Venkataraman, A., A. A. Nyblade, and J. Ritsema (2004), Upper mantle Q and thermal structure beneath Tanzania, East Africa from teleseismic P wave spectra, *Geophys. Res. Lett.*, *31*, L15611, doi:10.1029/2004GL020351.

Watson, T. (2005), The upper mantle structure beneath the Transantarctic Mountains and East Antarctic Craton using body-wave tomography, M.S. thesis, 91 pp., Pa. State Univ., Univ. Park.

Widmer, R., G. Masters, and F. Gilbert (1991), Spherically symmetric attenuation within the Earth from normal mode data, *Geophys. J. Int.*, *104*, 541–553.

S. Anandakrishan, A. A. Nyblade, and D. Voigt, Department of Geosciences, Pennsylvania State University, University Park, PA 16802, USA.

J. F. Lawrence, Institute of Geophysics and Planetary Physics, Scripps Institution of Oceanography, La Jolla, CA 92093–0225, USA. (jlawrence@ucsd.edu)

P. J. Shore and D. A. Wiens, Department of Earth and Planetary Sciences, Washington University, St. Louis, MO 63130, USA.